Computer Simulations Aimed at Exploring Protein Aggregation and Dissociation

Phuong H. Nguyen, Philippe Derreumaux

Computer Simulations Aimed at Exploring Protein Aggregation and Dissociation.

Phuong H. Nguyen,[1,2] Philippe Derreumaux[1,2*]

[1] CNRS, Université de Paris, UPR 9080, Laboratoire de Biochimie Théorique, 13 rue Pierre et Marie Curie, F-75005, Paris, France

[2] Institut de Biologie Physico-Chimique, Fondation Edmond de Rothschild, PSL Research University, F-75005, Paris, France

Abstract. Protein aggregation can lead to well-defined structures that are functional, but is also the cause of the death of neuron cells in many neurodegenerative diseases. The complexity of the molecular events involved in the aggregation kinetics of amyloid proteins and the transient and heterogeneous character of all oligomers prevent high-resolution structural experiments. As a result, computer simulations have been used to determine the atomic structures of amyloid proteins at different association stages as well to understand fibril dissociation. In this article, we first review the current computer simulation methods used for aggregation with some atomistic and coarse-grained results aimed at better characterizing the early-formed oligomers and amyloid fibril formation. Then we present the applications of non-equilibrium molecular dynamics simulations to comprehend the dissociation of protein assemblies.

Key words: amyloid, aggregation, structure, dynamics, thermodynamics, computer equilibrium and non-equilibrium simulations, all-atom, coarse-grained force field, aqueous solution, lipid membrane bilayer.

1. Introduction

Several diseases affect the central nervous system as the result of the aggregation of amyloid proteins. These diseases include Alzheimer's disease (AD) where the Aβ proteins of 39-43 amino acids and the tau protein ranging from 352 to 441 amino acids are the main players; Parkinson, where the α-synuclein protein of 140 amino acids is the main culprit; and prion diseases, with the implication of the prion protein spanning the amino acids 90-231 [1,2]. It is remarkable that these proteins sharing no amino acid sequence identity form amyloid fibrils *in vitro* and in the brain. Also, a disordered monomeric structure is not mandatory for amyloid fibril formation as the prion protein consists of a flexible N-terminal region (amino acids 90-122) followed by a three α-helix bundle with a small β-sheet [3]. Accumulation of amyloid aggregates is the result of an imbalance between their formation and removal. Aggregates and fibrils should be degraded by the lysosomal and proteasomal machineries [4], but some impairment is present [5].

The aggregation kinetics of amyloid proteins in aqueous solution, as measured by Thioflavin fluorescence, displays a sigmoidal curve with a lag-phase where monomers self-assemble into oligomers until the growth phase where the fibril elongates, followed by the saturation phase where the system is in equilibrium between fibrils and a low concentration of monomers. Amyloid formation goes beyond classical nucleation theory where primary nucleation is sufficient, and all models include secondary nucleation such as fibril fragmentation and fibril surface-catalyzed effects [6,7]. In these mathematical models, all events, except fragmentation, involve association/dissociation of one monomer to/from an assembly [6].

Experimental determination of amyloid structures at all aggregation steps is very challenging due to the intrinsic disorder of the proteins and the heterogeneous ensemble of all species along the amyloid fibril formation pathways. At the monomer level, there is CD (circular dichroism) and NMR (nuclear magnetic resonance)

evidence that Aβ40 and Aβ42 peptides are fully disordered with mainly turn/coil and only transient secondary structures in aqueous solution [8]. The addition of the residues 41-42 changes the equilibrium ensemble as deduced from NMR. Both tau and α-synuclein monomers are unstructured in solution and mammalian cells [9,10].

At an oligomer level, Yu *et al.* carried out solution NMR on N-Met-Aβ42 (additional M residue on the N-terminus) tetramers in sodium dodecyl sulfate (SDS) micelles, with 0.2% SDS in weight. The model displays an intra-peptide antiparallel β-hairpin spanning residues 17-23 and 28-33, and inter-peptide parallel β-sheet contacts formed by residues 34-42. Overall, all NMR-derived oligomer models up to 30 Aβ peptides point to transient anti-parallel β-states with in some cases intra-molecular β-hairpin, in agreement with FTIR experiments [2,11]. We are lacking oligomer structures of tau and α-synuclein in aqueous solution, though stable toxic oligomers of α-synuclein have been characterized by cryo-electron microscopy (c-EM) [12].

Based on solid-state NMR experiments, Aβ42 fibrils *in vitro* show intra-peptide U-shape with two β-strands or S-shape with three β-strands and different inter-peptide interfaces. Fibrils of synthetic Aβ40 peptides have β-strands at residues 10-23 and 30-38 with the N-terminal residues disordered. However, fibrils made of AD-brain-derived Aβ40 peptides displays a deformed intra-peptide U-shape conformation, with a twist at residues 19-23, a kink at residue 33, and a bend at residues 37-38 and a more ordered N-terminus [2,13]. The amyloid structures of recombinant α-synuclein [14], and tau filaments from the brain of an individual with AD [15] at the resolution of 0.30-0.35 nm were determined by c-EM. For tau, filament cores consist of two identical protofilaments comprising residues 306-378, and adopting a combined cross-β/β-helix structure. Paired helical and straight filaments differ in their inter-protofilament packing and are ultrastructural polymorphs [15]. For α-synuclein, the regions 37-99 folds into a β-strand-rich architecture with a Greek-key-like topology [14].

Albeit Aβ40 and Aβ42 peptides are the main component of senile plaques,

there is no correlation between number of amyloid deposits and the severity of the disease. It has been demonstrated that oligomers from the dimer to at least 12-mers are believed to be the main culprits of AD, initiating a series of events leading to neuronal death (amyloid cascade hypothesis), but the mechanisms underlying the neurotoxicity of Aβ oligomers are still elusive [16]. There is also experimental evidence that soluble tau and α-synuclein oligomers are the most toxic. Characterization of all these oligomers at atomistic level is also difficult because amyloid formation is very sensitive to experimental conditions (pH, temperature peptide concentration, external force applications from agitation, electric field, shear, etc.), and environmental conditions (presence of membrane, metal ions, crowding) [2,17].

To complement experiments and provide a detailed description of the aggregation process, computer simulations are ideal tools though limitations persist and explain the emergence of new sampling methods, refined potential energy functions and a wide range of protein representations. Section 2 reviews these aspects to capture the conformational ensemble of intrinsically disordered proteins at different aggregation stages and presents some simulation results on small oligomers of amyloid peptides in solution and lipid membrane bilayers. Section 3 focuses on non-equilibrium MD simulations and reports on their applications to amyloid fibril and virus dissociation.

2. Computer simulations of amyloid protein aggregation

Three ingredients are required for performing computer simulations. First, we need a description of the system: all-atom with explicit solvent or implicit solvent (e.g., Generalized Born) model or a coarse-grained (CG) model with various numbers of internal degrees of freedom restricted or not on a lattice. Then, we need an accurate description of the intra-molecular and intermolecular interactions described by a potential energy function. Third, a method to sample the microstates of the system is necessary, a microstate being a set of given coordinates and moments (r_n, p_n) of all particles of the system. For a system of N particles, we have a

6N-dimension phase space and a 3N-dimension configuration space. All microstates do not have, however, the same importance for computing macroscopic properties. This configuration space or landscape is characterized by an exponential number of low-energy conformations or minima that are connected by energy barriers or saddle points of several to many times k_BT at room temperature.

Given the potential energy function, statistical physics tell us two principles: (a) ensemble averages; thermodynamic properties are averages of microscopic quantities over the accessible microstates of the system, and (b) ergodicity; it is equivalent to compute the time average (by molecular dynamics) or the statistical average of the quantity (by Monte Carlo). Of course, the accessible microscopic states depend on the external parameters applied and the probabilities of microstates depend on the ensembles (NVE microcanonical ensemble, NVT canonical ensemble, NPT isothermal-isobaric ensemble and μVT grand-canonical ensemble). But we know that the partition function contains all the information necessary to compute average quantities, and over all possible configurations, only few have a non-negligible contribution to the partition function. We now review the methods to sample the microstates of protein/peptide oligomers.

2.1. Monte-Carlo simulations

The principle of Monte Carlo (MC) simulation is to generate conformations either randomly, using simple motion rules (such as rigid body translations, rotations of a set of chains, torsional change of one amino acid) or guided by some information. Then, the new conformation is accepted if the Metropolis criterion is satisfied [18]. The principle of replica exchange MC (REMC) simulation is to run multiple MC simulations at various temperatures in parallel and exchange consecutive replicas according to the Metropolis criterion [19].

Rosetta uses a five-bead representation that includes the backbone heavy atoms and a centroid located at the side-chain center of mass, followed by an all-atom representation. Rosetta uses a MC fragment assembly of nine residues and

then three residues to identify the lowest-energy states. The CG energy function includes many terms such as hard sphere repulsion, side-chain packing, secondary structure packing, and Ramachandran torsion angle filters, among others. Short-range and long-range backbone–backbone hydrogen bond energy terms are only used during the full-atom refinement. This two-step Rosetta procedure enables structure prediction with atomic level accuracy for small proteins [20]. Building on this framework, Baker *et al.* developed a general method for a simultaneous prediction of protein folding and docking of multiple-chain systems at high resolution [21]. This method was applied with new solid-state NMR data to design a barrel hexamer as building block of Aβ40 protofibrils. The core of the oligomers consists of all residues of the central and C-terminal hydrophobic regions. The model explains why Aβ42 forms oligomers and protofibrils more easily than Aβ40 [22].

Irback *et al.* developed the PROFASI model based on an all-atom model with an implicit solvent, and coupled it to MC. The potential energy function takes into account excluded volume effects, local electrostatic along the backbone, backbone and side chain hydrogen bonds and a final term for side chain charge-charge interactions, and hydrophobic effect. They studied the aggregation of 3 systems consisting of 12, 24 and 26 peptides of the six residue PH6 fragment from the tau protein. The largest aggregates are composed of two twisted β-sheets, but have a mixed parallel/antiparallel β-strand organization vs. parallel β-strands in fibrils. The fraction of parallel β-sheet increases, however, with aggregate size [23].

On-lattice MC and REMC simulations have investigated the nucleation mechanisms [24-26], the free energy landscapes (FEL) of oligomers of the Aβ16-22 and Aβ35-42 peptides [27,28], and the nucleus size of Aβ42 [29]. Li *et al.* developed a protein model with a simple hydrophobic/neutral/hydrophilic energy model. MC simulations of multiple Aβ42 chains, each chain consisting of eight residues, showed that the nucleus size N* is 11 chains [29,30]. Frenkel *et al.,* by developing a sophisticated lattice model that considers the formation of H-bonds, the directions of side-chains and pairwise interaction energies between all amino acids, were able to

capture amyloid fibril formation for a designed 7-residue peptide [31].

We introduced the CG OPEP force field into Frenkel's lattice model to explore the nucleus size of real amyloid peptides. The OPEP (optimized potential for efficient peptide structure prediction) model consists of one bead per side-chain and the N, H, Cα, C and O atoms. A particularity of OPEP is that it includes two-body and four-body H-bonds along with side chain interactions [32,33]. Using REMC simulations of 10, 20, 30 chains of the Aβ37-42 peptide, the results show that, at the folding temperature of the monomer, aggregates of 10 and 20 peptides are mainly amorphous, with a small population of native fibrils characterized by parallel β-strands and antiparallel β-sheets. Moving to 30 peptides, the FEL changes with a much lower population of disordered aggregates, a high population of native fibrils and the formation of β-rich structures capturing fibril elongation and secondary nucleation processes [28].

Tau441 monomer conformation was determined from MC, a CG model with only repulsive Lennard-Jones interactions, and inter-residue distances obtained from single molecule fluorescence resonance energy transfer [34]. The structural characteristics of intrinsically disordered proteins of residues varying between 20 to 441 were also studied by MC with a two-bead model per amino acid [35].

2.2 Activated methods

An approach to accelerate the search of microstates of lowest energy is to use activated methods. The Activation-Relaxation Technique (ART) generates pathways connecting adjacent local minima via first-order saddle points [33]. ART coupled to the OPEP CG force field enabled the identification of key metastable states for amyloid monomer (Aβ21-30) and oligomers (Aβ16-22 and KFFE) [36-39]. Wales *et al.* used basin-hoping global optimization coupled to discrete path sampling to generate disconnectivity graphs of the all-atom Aβ17-42 monomer and pentamers in implicit solvent [40].

2.3 MD simulations

Atomistic molecular dynamics (MD) simulations in explicit solvent offer the most detailed picture of protein folding and aggregation. Nguyen *et al.* revealed by using 0.34 millisecond MD that the probability of the amyloid-competent state of the Aβ16-22 dimer is at most of 10% using the most recent atomistic force fields (CHARMM36m/TIP3P-modified [41] and AMBER99sb with disp, [42] a TIP4P modified water) [43]. Strodel *et al.* carried out MD simulations of 20 Aβ disordered chains in implicit solvent on the microsecond time scale followed by transition networks analysis. They revealed that the Aβ40 and Aβ42 aggregation pathways depend on oligomer shapes with compact and extended configurations [44]. MD simulations of Aβ oligomers in explicit solvent with the H6R and D7N mutations provided insights into the contribution of the loop region (residues 23-28) [45,46]. The impact of mutations and N-terminal truncation on amyloid pores made of double layers of Aβ peptides with U-shaped conformations was investigated in lipid membrane bilayers [47,48]. Computational insights into lipid assisted peptide misfolding and aggregation in neurodegeneration was recently reviewed [49].

The longest simulation performed thus far on the Anton computer, designed for MD only, reached 1 millisecond for protein folding using atomistic force field in explicit solvent [50]. This fast computer also allows an atomic-level description of protein-protein association [51]. In the case of amyloids, the monomeric ensemble of α-synuclein, generated by Anton using AMBER99sb-disp force field, is mainly coil/turn and its radius gyration distribution displays two peaks centred at 2.5 and 4.0 nm with a mean value at 3.7 vs. 3.1 nm by experimental means [42].

To accelerate sampling of amyloid oligomer and amyloid fibril formation, while preserving approximate dynamics, we can resort to Langevin dynamics (LD) simulations with CG models in explicit or implicit solvent. Xu *et al.* studied the assembly of the Aβ17-42 peptides in the presence of fibrils by using the CG protein Martini force field in explicit CG water model where the residues 18-26 and 31-42 are set to remain in a β-strand [52]. Using a two-state model for each peptide and LD, Caflisch *et al.* found that the nucleus size varies between 4 and 35 depending

on the energy difference between the amyloid-competent and amyloid-protected states [53]. By using LD and a three-bead model (two for the backbone, and one for the side-chain) along with a simple energy function that controls the β-strand propensity of each peptide, Shea *et al.* found that the oligomers consist of disordered aggregates, multiple β-sheet layers with different orientations including the cross-β structure and β-barrels, when the β-strand propensity is not too high [54]. This ensemble is consistent with other CG simulations [55,56]. Finally, Scheraga *et al.* used their CG united-residue UNRES force field to study the aggregation of 5 Aβ1-28 peptides [57].

While MD and LD integrate Newton's equations of motion with a time step of 2 ns for atomistic systems, DMD (discontinuous MD) simulations are event-driven and keep track of the positions and velocities of all particles at collision times. DMD is several orders of magnitude faster than MD for a CG model, but requires spherically symmetric potentials consisting of square wells between particles. DMD was coupled to all-atom model with implicit solvent [58], and CG models such as PRIME20 [59].

Using all-atom DMD, Feng *et al.* demonstrated the non-negligible probability (2-4%) of β-barrel formation for Aβ16-22 [58]. The four-bead "Urbanc" and PRIME20 models use three spheres for the N, Cα, and CO backbone atoms and one bead for the side chain. Using CG DMD, differences in oligomer size distributions between the Aβ40 and Aβ42 peptides were found consistent with experimental data [60]. CG DMD simulations show that the secondary nucleation mechanism is dominant in Aβ40 fibril formation when mixed with Aβ16-22, even if the primary/secondary nucleation and growth processes occur at the same time [59]. Dokhloyan and collaborators provided insights into the unstructured conformation of the tau441 and α-synuclein monomers by atomistic DMD simulations guided by structural proteomics data resulting from short-range cross-linkers (reagents) and mass spectrometry experiments [61,62].

We emphasize that an implicit solvent model neglects hydrodynamics interactions that play significant effects in modelling amyloids and lipid systems [63,64].

2.4 Guided MD simulations

Enhanced sampling is performed in metadynamics by an external history-dependent bias potential affecting few collective variables (CV). The bias is adaptively constructed as a sum of Gaussians deposited along the system trajectory to prevent the system from revisiting previous conformational regions. Although simple in principle, finding an effective set of collective variables is not a trivial task using all-atom models and explicit solvent. For the Aβ40 monomer, three CV's are sufficient, the anti-parallel β-sheet and α-helix contents, and the number of hydrophobic contacts [65]. For a system of 18 Val8 peptides, eight CV's were used, some being complex. The free energy landscape projected on three CV's showed that the maximum free energy is characterized by a transition from mixed parallel/antiparallel to parallel β-strand orientations, and the free energy decreases as soon as a sufficient number of parallel sheets is formed [66].

Recently, Noé et al. opened a new way by training a deep neural network to explore rugged potential energy landscapes for MD folding of model systems in implicit solvent and obtaining accurate free energy differences between key metastable states [67]. The challenges to obtain such precise information for amyloid aggregates might be solved soon combining REMD and machine learning.

2.5 REMD

Replica exchange MD (REMD) simulations are the most currently used method for amyloid fibril formation, even if they are very sensitive to the overlap between the replica total energies, the energy overlap scaling with the number of particles as $N^{-1/2}$. Optimal exchange rate between replicas requires therefore many trajectories in parallel. All-atom REMD simulations in explicit solvent have been

performed on many systems. These studies revealed the change in the intrinsic disorder properties of Aβ40 and Aβ42 upon mutation at position 2 [68-71]. The stability of Aβ11-40 trimer in parallel and antiparallel β-sheet conformations was also investigated in solution and in lipid bilayers [72]. WT Aβ oligomers with multiple drugs revealed interactions that are very short time and transient [73-77]. The mechanisms of graphene oxide nanosheet [78] and carbon nanotube [79,80] inhibition of Aβ peptides were also disclosed.

We designed 3D structures of Aβ40 and Aβ42 β-barrels in a bilayer mimicking a neuronal membrane [81]. The atomistic REMD simulation of the tetramer model in a bilayer mimicking a neuronal membrane provide new insights into the amyloid pore hypothesis and explains the higher toxicity of Aβ42 than its Aβ40 counterpart. We also reported novel findings as the stability of this Aβ40/42 β-barrel in aqueous solution [82] and the stability of Aβ42 barrel with the D23N and A2T mutations [83].

The number of solvent molecules limits the optimal exchange rate between replicas in REMD. As protein-protein and protein-solvent interactions are dominant in protein recognition, [84] focusing on these interactions rather than solvent-solvent interactions is of interest. Simulation schemes based on potential energy rescaling and Hamiltonian replica exchange such as replica exchange with solute tempering (REST) and H-REMD have also been used [84-86]. As an example, comparison of REST and standard REMD simulations to study the Aβ25-35 peptide in water and a system consisting of two Aβ10-40 peptides binding to a DMPC lipid bilayer shows high speed CPU gain with the number of replicas reduced four to five times, while the number of unique states is very similar between the two simulations [86].

Finally, in addition to REMD simulations based on coarse-grained models [34], hierarchical procedures are often employed for multiple purposes. One common scheme is to start with CG MD/REMD (in solution or membrane), followed a refinement by all-atom MD [85,87-90].

2.6 Simulated tempering

In simulated tempering (ST), temperature is a dynamical variable with discrete values T_n, and the canonical Boltzmann distribution is replaced by a generalized canonical distribution $W_{ST}(E,\beta_m) = exp(-\beta_m E + f_m)$. If the weight parameters f_m are chosen such that the distribution of temperature is flat, then a random walk in temperature and potential energy spaces is realized, allowing escape from all local energy minima. A common strategy to estimate the weights is to perform short trial MD simulations from average potential energies [91-94], or via multiple-histogram reweighting [95-97]. Using this strategy, Favrin *et al.* studied the aggregation of six Aβ16-22 peptides using a sequence-based atomic protein model, and found different aggregates with a high β-sheet content [98].

We developed a ST scheme with on-the-fly weight determination [99]. Simulation starts with zero values for the weight parameters, and they are updated on-the-fly as the simulation progresses by the trapezoid rule [94]:

$$f_{n+1}(t) = f_n(t) + \frac{(\beta_{n+1} - \beta_n)\left(\overline{E}_{n+1}(t) + \overline{E}_n(t)\right)}{2},$$

where $E_n(t)$ is the accumulated potential energy up to time t and $\beta=1/k_BT$. This simulated tempering method was compared to REMD on the Aβ16-22 trimer using the OPEP CG force field [99], and the folding of the 20-residue Trp-cage using atomistic force field in explicit solvent [100]. Figure 1 shows the distribution of the nematic order parameter P_2 for Aβ16-22 trimer at 300 K obtained from 400 ns ST and 100 ns REMD trajectories. In both simulations, 20 temperatures spanning 280-500 K were used. The ST configuration distribution is in excellent agreement with that obtained from REMD but with a much lower CPU cost. The trimer samples configurations with one peptide moving around an antiparallel β-sheet ($P_2 \approx 0.3$), and an antiparallel three-stranded β-sheet ($P_2 \approx 0.7$), fully consistent with atomistic simulations [101]. Note, we can use multiple atomistic force fields into a single

simulated tempering run [102].

3. Non-equilibrium MD simulations towards understanding amyloid fibril dissociation and virus dissociation

Although our knowledge on amyloid fibril formation, no drugs are currently available to stop or retard the propagation of Alzheimer's disease [103]. It is interesting that evolution produces amyloids for diverse functional purposes including protein storage, silk formation, melanin production, immune response and biofilm formation. For instance, peptide hormones are stored in the form of amyloids and released to the extracellular space upon the action of an appropriate trigger.

Amyloid fibrils often exhibit unusual material properties, such as pull strength comparable to that of steel, mechanical shear stiffness similar to that of silk, as well as extreme persistence length and mechanical rigidity [104,105]. As a result, they have been exploited for novel biological materials [106]. While current research focuses on the fabrication and applications of peptide nanotubes, a few studies are carried out to address how to dissociate these extremely robust materials without damaging the surrounding environment. Clearly, it is important to understand the amyloid fibril disassembly mechanisms in details.

Experimentally, amyloid fibrils can be dissociated with chemicals such as guanidine hydrochloride or dimethyl sulfoxide [107], but these chemicals are highly toxic and harmful. There have been suggestions to include within proteins molecular photo-switches such as azobenzene chromophore. This guarantees that the light-induced structural changes of the chromophore upon photo-isomerization are directly transferred into the peptide chain, switching the peptide from the favorable to unfavorable aggregation-prone states, resulting in protein disassembly [108-111]. Kawasaki *et al.* demonstrated the disassembly amyloid fibrils with mid-infrared laser [112-115]. To this end, they developed a free-electron laser having specific oscillation characteristics of a picosecond pulse structure, a tunable wavelength

within infrared frequencies and a high photon density. Tuning the laser frequency to that of the amide I band involving C=0 stretching, they were able to dissociate amyloid fibrils into soluble monomers, including fibrils of lysozyme and of a short peptide of the thyroid hormone.

Leinenga *et al.* utilized a repeated scanning ultrasound in combination with intravenous injection of micro-bubbles to remove cerebral amyloid depositions in mouse brain [116]. They postulated that albumin entry into brain parenchyma via an opened blood-brain-barrier could mediate Aβ uptake by microglia. By using *in vitro* experiments, Goto *et al.* showed that ultrasonication accelerates the depolymerization of fibrils into monomers [117,118]. It was postulated that the inertial cavitation might occur and disrupt the fibrils. This suggests that the reduction of amyloid deposits observed by Leinenga *et al.* could also be due to the direct interaction of ultrasound and amyloid plaque that leads to small soluble species and facilitates efflux of Aβ into peripheral circulation.

Theoretically, we have developed a comprehensive laser-induced non-equilibrium molecular dynamics (NEMD) simulation method, and applied it to study the molecular mechanism of the dissociation process observed by experiments of amyloid fibrils [119]. The method was also applied to study the disassembly of other structures including peptide nanostructures [120], DNA duplex and viruses [121], and cellulose [122]. In this method, a time-dependent electric field

$$E(t) = E_0 exp\left[-\frac{(t-t_0)^2}{2\sigma^2}\right] cos[2\pi c\omega(t-t_0)],$$

is applied to the system to mimic a laser pulse. Here, E_0 represents the amplitude of the electric field, σ is the pulse width, t is the time after the pulse maximum t_0, c is the speed of light and ω is the frequency. Figure 2, shows, as an example, a chain of 10 laser pulses. Several technical details must be taken care. In a conventional MD simulation, the temperature of the system is typically maintained by rescaling the velocities of all atoms at every time step. In a laser-induced non-equilibrium

experiment, on the other hand, the photo-excitation results in a vibrationally hot molecule, which is then cooled via the transfer of the vibrational energy to the surrounding solvent molecules [123]. Thus, in our NEMD simulations only the waters are coupled to the heat bath in order to maintain the temperature of 310 K with a coupling constant of 0.1 ps. This also mimics the experimental conditions, in which water is added periodically to the suspension during the irradiation process in order to prevent excessive evaporating [112-115]. Also, to ensure stability, a short time step of 0.2 fs was used.

Figure 3 shows the snapshots of the GNNQQNY fibril during the NEMD simulation irradiated by 10 laser pulses, with a pulse duration of 10 ps, intensity $E_0 = 2$ V/nm and frequency ω = 1675 cm^{-1}[124]. We find that this laser frequency is resonant with the amide I mode of the β -sheet structure [125], thus the β -sheet is quickly dissociated, whereas the surrounding peptides mainly in coli/turn, are hardly affected. Interestingly, the dissociation process is initiated at the interior of the fibril and then propagates to the outer. To make a connection to experiment, we calculate the WSAXS spectra for these selected structures. Within the first 20 ps, the fibril structure is well maintained, the peak of the spectrum locates at $q = 13.3$ nm^{-1} which is very close to the peak at 12.8 nm^{-1} of the experimental spectrum. Both peaks correspond to the inter-chain distances of 0.47 and 0.49 nm in the simulated and experimental fibril structures, respectively. Upon laser irradiation, the peak is shifted to $q = 12.5$ nm^{-1} and $q = 11.5$ nm^{-1} at 22 ps and 24 ps, respectively. The snapshots at these times indicate that the β -sheets are still maintained, and only chains, especially at the middle, are more separated apart. At 26 and 30 ps, the height of the peaks is reduced due to the fact the fibril structure is partially destroyed. After the first pulse, t>50 ps, the spectrum basically does not exhibit any specific peaks, confirming that the fibril structure is completely dissociated.

The laser method has been successfully used to dissociate amyloid fibrils. Some other nanostructures such as viruses are also assembled from repeating

protein subunits to form highly symmetrical and stabilized by a highly cooperative nature of the hydrogen bond network. Thus, we also show as a proof-of-concept that infrared laser can also dissociate virus [121]. This may open a new, efficient way to cleave or to recycle virus-based material, provide an extremely valuable tool to elucidating mechanical aspects of viruses, and play an important role in solving virus-related diseases. Adopting the Poliovirus as a representative example, the NEMD laser-induced simulation shows that the primary step in the dissociation process is due to the strong resonance between the amide I vibrational modes of the virus, and the tuned laser frequencies. The process is determined by a balance between the formation and dissociation of the protein shell, reflecting the highly plasticity of the virus. Our method should also provide a feasible approach to simulate viruses, which is too time-consuming for conventional equilibrium all-atom MD simulations.

The impact of ultrasound wave on amyloid fibrils was studied using all-atom NEMD simulation by Okumura and Itoh [126], with a time-dependent sinusoidal pressure of the form

$$P(t) = P_0 + \Delta P \sin\left(\frac{2\pi t}{\tau}\right)$$

where P_0 is initial pressure, ΔP is the pressure amplitude and τ is the ultrasound wave period. The authors studied fibrils formed by twelve, six and three Aβ17-42 peptides with amplitude of ultrasound of 200 MPa and period of 1 ns. The simulations show that, when pressure is negative, a bubble is formed around the hydrophobic residues, and most chains maintain their secondary structures in the bubble. When the pressure is positive, fibril dissociation occurs. Therefore, the dissociation mechanism is essentially due to the presence of an empty water space around the hydrophilic residues. Direct interaction between jet flows and the fibril was not shown in their study. Longer irradiation times are required to break short fibril models, because they do not many hydrophobic residues to serve as a nucleus to form a bubble.

In many biological applications, bubble collapse must be controlled to avoid the damage of biomolecules, and stable oscillation of bubbles, called stable cavitation, is preferable. This can happen when the ultrasound is weak and the bubble oscillation amplitude is small. The bubbles could be naturally formed inside the system or injected to the system, and oscillate harmonically during the ultrasound irradiation. To simulate bubble stable oscillation, we developed a NEMD method [127,128], where a bubble is represented by a particle with low mass and no charge and interacts with the surrounding waters by a time-dependent Lennard-Jones potential:

$$V[r,\sigma(t)] = 4\epsilon\left[\left(\frac{\sigma(t)}{r}\right)^{12} - \left(\frac{\sigma(t)}{r}\right)^{6}\right],$$

where *r* is the distance between the center of the bubble and the oxygen atom of a water molecule and $R(t) \equiv \sigma(t)$ is the bubble radius. To mimic the stable expansion and contraction of the bubble, the time-dependent bubble radius is expressed as a harmonic function:

$$R(t) = \frac{(R_{max} + R_{min})}{2} + \frac{(R_{max} - R_{min})}{2} cos\left(\frac{2\pi t}{\tau} + \pi\right),$$

where τ is the vibrational period of the bubble radius, and the bubble radius of the varies between R_{min} at $t = n\tau$ and R_{max} at $t = \left(n + \frac{1}{2}\right)\tau$ with n=0, 1.. the periodicity. This way, the time-dependent potential changes harmonically during the simulation, pushing and pulling waters back and forth and mimicking the bubble stable cavitation.

Because the bubble cavitation is a not an equilibrium process, an important issue is whether the simulation should use NVT (constant number of atoms N, volume V and temperature T) or NPT (constant number of atoms N, pressure P and temperature T) ensemble. In a conventional MD simulation, the pressure of the system is typically maintained at a constant by rescaling the box lengths at every

time step. In experiments, the sound wave results in an oscillation pressure across the system. This suggests that our non-equilibrium MD simulation should be carried out in the NVT ensemble, where the pressure is allowed to change.

We employ this method to simulate the effects of stable bubble cavitation on an amyloid fibril model formed by five Aβ17-42 peptides in TIP3P water containing 3% bubbles [127]. The bubble radius is allowed to vibrate with a period $\tau = 50$ ps and amplitudes $R = 0.2 - 0.6$ nm. Simulation shows that the expansion and contraction of bubbles change the water density around the fibril, inducing fluctuations in the water pressure exerted on the fibril, and this periodically change in water pressure leads to the dissociation of the whole fibril. Figure 4 shows three selected. Initially, the fibril forms a very stable cross-β structure (orange segments) stabilized by backbone hydrogen bonds. Under the stable bubble cavitation, the fibril is partially dissociated with chains still in β-hairpin-like structures, but separated apart, allowing a few bubbles to enter the fibril interior. These interior bubbles exert efficiently water pressure on the fibril from inside, destroy the β-hairpins, convert chains into the random coil monomers and eventually dissociate the whole fibril after 100 periods (t=5000 ps). We should mention that in these simulations, only 3% of bubbles are in the box, and we find that bubbles do not make any direct contact with the fibril, neither with hydrophobic nor hydrophilic residues. This confirms that our dissociation mechanism is not due to the destabilization of the fibril induced by the air-water bubble interface around hydrophilic residues as reported in the simulations of Okumura *et al.* [124]. Taken together, the physics under fibril dissociation mechanisms induced by ultrasound and bubble stable cavitation is quite different.

4. Conclusions

We have reviewed some results of computer simulations aimed at exploring protein aggregation and dissociation, focusing essentially on the amyloid-β oligomers and fibrils. Computational results on other amyloid proteins can be found in Ref. [129-133]. More accurate force fields at atomistic and different levels of

coarse-grained and new sampling approaches are being developed for IDP's, and simulations closer to *in vivo* conditions are being explored [41,42,134-147].

Many molecules targeting amyloid-β oligomers have failed to cure Alzheimer's disease [103,148], and this failure raises a number of questions about the amyloid cascade hypothesis [16]. Perhaps we may take into account a multi-target strategy and the role played by mitochondrial membranes in the context of AD and other neurodegenerative diseases [149].

AUTHOR INFORMATION

Corresponding Author

E-mail: philippe.derreumaux@ibpc.fr

ORCID

Phuong H. Nguyen: 0000-0003-1284-967X

Philippe Derreumaux: 0000-0001-9110-5585

Notes

The authors declare no competing financial interest.

ACKNOWLEDGMENTS

We acknowledge support by the "Initiative d'Excellence" program from the French State (Grant "DYNAMO", ANR-11-LABX-0011-01, and "CACSICE", ANR-11-EQPX-0008).

REFERENCES

(1)Dobson CM, Knowles TPJ, Vendruscolo M (2019) The Amyloid Phenomenon and Its Significance in Biology and Medicine. Cold Spring Harb Perspect Biol. pii: a033878.

(2) Nasica-Labouze J, Nguyen PH, Sterpone F et al. (2015) Amyloid beta protein and Alzheimer's disease: when computer simulations complement experimental studies. Chem Rev 115:3518–3563.

(3)Caldarulo E, Barducci A, Wüthrich K, Parrinello M (2017) Prion protein *β*2-*α*2 loop conformational landscape. Proc Natl Acad Sci U S A 114:9617-9622.

(4)Cliffe R, Sang JC, Kundel F, Finley D, Klenerman D, Ye Y (2019) Filamentous Aggregates are Fragmented by the Proteasome Holoenzyme. Cell Rep. 26: 2140-2149.e3.

(5) Deger JM, Gerson JE, Kayed R (2015) The interrelationship of proteasome impairment and oligomeric intermediates in neurodegeneration. Aging cell. 14: 715-724.

(6) Banks HT, Doumic M, Kruse C (2017) A numerical scheme for the early steps of nucleation-aggregation models. J Math Biol 74:259-287.

(7) Dammers C, Schwarten M, Buell AK et al (2017) Pyroglutamate-modified Aβ(3-42) affects aggregation kinetics of Aβ(1-42) by accelerating primary and secondary pathways. Chem. Sci 8:4996.

(8) Roche J, Shen Y, Lee JH et al (2016) Monomeric Aβ(1-40) and Aβ(1-42) Peptides in Solution Adopt Very Similar Ramachandran Map Distributions That Closely Resemble Random Coil. Biochemistry 55:762-765.

(9) Schwalbe M, Ozenne V, Bibow S, Jaremko M, Gajda M, Jensen MR, Biernat J, Becker S, Mandelkow E, Zweckstetter M, Blackledge M (2014) Predictive atomic resolution descriptions of intrinsically disordered hTau40 and alpha-synuclein in solution from NMR and small angle scattering. Structure 22: 238-249.

(10) Theillet FX, Binolki A, Bekei B, Martorana A, Rose HM, Stuiver M, Verzini S, Lorenz D, van Rossum M, Goldfarb D, Selenko P (2016) Structural disorder of alpha-synuclein persists in mammalian cells. Nature 530: 45-50.

(11) Nagel-Steger L, Owen MC, Strodel B (2016) An Account of Amyloid Oligomers: Facts and Figures Obtained from Experiments and Simulations. Chembiochem 17:657-76.

(12) Chen SW, Drakulic S, Deas E, Ouberai M, Aprile FA, Arranz R, Ness S, Roodveldt C, Guilliams T, De-Genst EJ et al. (2015) Structural characterization of toxic oligomers that are kinetically trapped during alpha-synuclein fibril formation. Proc Natl Acad Sci U.S.A. 112: E1994-2003.

(13) Kreutzer AG, Nowick JS (2018) Elucidating the Structures of Amyloid Oligomers with Macrocyclic beta-Hairpin peptides : Insights into Alzheimer's Disease and Other Amyloid Diseases. Acc. Chem. Res 51: 706-718.

(14) Li Y, Zhao C, Luo F et al (2018) Amyloid fibril structure of α-synuclein determined by cryo-electron microscopy. Cell Res 28:897-903.

(15) Fitzpatrick AWP, Falcon B, He S et al (2017) Cryo-EM structures of tau filaments from Alzheimer's disease. Nature 547:185-190.

(16) Selkoe DG, Hardy J (2016) The amyloid hypothesis of Alzheimer's disease at 25 years. EMBO Mol. Med. 8:595-608.

(17) Owen MC, Gnutt D, Gao M et al (2019) Effects of in vivo conditions on amyloid aggregation. Chem Soc Rev 48:3946-3996.

(18) Derreumaux P (2001) Generating Generating ensemble averages for small proteins from extended conformations by Monte Carlo simulations. Phys Rev Lett 85:206-209.

(19) Levine ZA, Shea JE (2017) Simulations of disordered proteins and systems with conformational heterogeneity. Curr Opin Struct Biol 43:95-103.

(20) Bradley P, Misura KM, Baker D (2005) Towards high-resolution de novo structure prediction for small proteins. Science 309:1868–1871.

(21) Das R, Andre I, Shen Y et al (2009) Simultaneous prediction of protein folding and docking at high resolution. Proc Natl Acad Sci U S A 106:18978–18983.

(22) Lendel C, Bjerring M, Dubnovitsky A et al (2014) A hexameric peptide barrel as building block of amyloid-β protofibrils. Angew Chem Int Ed Engl 53:12756-12760.

(23) Li DW, Mohanty S, Irbäck A et al (2008) Formation and growth of oligomers: a Monte Carlo study of an amyloid tau fragment. PLoS Comput Biol 4:e1000238.

(24) Irback A, Jonsson S, Linnemann N et al (2013) Aggregate geometry in amyloid fibril nucleation. Phys. Rev. Lett 110: 058101.

(25) Šarić A, Michaels TCT, Zaccone A et al (2016) Kinetics of spontaneous filament nucleation via oligomers: Insights from theory and simulation. J Chem Phys. 145:211926

(26) Bieler NS, Knowles TP, Frenkel D et al (2012) Connecting macroscopic observables and microscopic assembly events in amyloid formation using coarse grained simulations. PLoS Comput Biol 8:e1002692

(27) Tran TT, Nguyen PH, Derreumaux P (2016) Lattice model for amyloid peptides: OPEP force field parametrization and applications to the nucleus size of Alzheimer's peptides. J Chem Phys 144:205103.

(28) Sterpone F, Doutreligne S, Tran TT et al (2018) Multi-scale simulations of biological systems using the OPEP coarse-grained model. Biochem Biophys Res Commu 498:296-304.

(29) Li MS, Klimov DK, Straub JE et al (2008) Probing the mechanisms of fibril formation using lattice models. J. Chem. Phys 129:175101.

(30) Co NT, Li MS (2012) New method for determining size of critical nucleus of fibril formation of polypeptide chains. J. Chem. Phys 137:095101.

(31) Abeln S, Vendruscolo M, Dobson C et al (2014) A simple lattice model that captures protein folding, aggregation and amyloid formation. PloS ONE 9: e85185.

(32) Wei GH, Derreumaux P, Normand M (2003) Sampling the complex energy landscape of a simple β-hairpin. J. Chem Phys. 119:6403-6406.

(33) Sterpone F, Melchionna S, Tuffery P. et al (2014) The OPEP protein model: from single molecules, amyloid formation, crowding and hydrodynamics to DNA/RNA Systems. Chem. Soc. Rev 43: 4871-4893.

(34) Nath A, Sammalkorpi M, DeWitt DC, Trexler AJ, Elbaum-Garfinkle S, O'Hern CS, Rhoades E (2012) The conformation ensemble of alpha-synuclein and tau: combining single-molecule FRET and simulations. Biophys. J. 103 : 1940-1949.

(35) Baul U, Chakraborty D, Mugnai ML, Straub JE, Thirumalai D (2019) Sequence effects on size, shape and structural heterogeneity in intrinsically disordered proteins. J Phys Chem B 123: 3462 – 3474.

(36) Santini S, Mousseau N, Derreumaux P (2004) In silico assembly of Alzheimer's Abeta16-22 peptide into beta-sheets. J. Am. Chem. Soc. 126:11509-11516.

(37) Melquiond A, Mousseau N, Derreumaux P (2006) Structures of soluble amyloid oligomers from computer simulations. Proteins 65:180-191.

(38) Melquiond A, Boucher G, Mousseau N et al (2005) Following the aggregation of amyloid-forming peptides by computer simulations. J Chem Phys. 122:174904.

(39) Chen W, Mousseau N, Derreumaux P (2006) The conformations of the amyloid-beta (21-30) fragment can be described by three families in solution. J Chem Phys 125:084911.

(40) Röder K, Wales DJ (2018) Energy Landscapes for the Aggregation of $A\beta_{17-42}$. J Am Chem Soc 140:4018-4027.

(41) Huang J, Rauscher S, Nawrocki G, Ran T et al (2017) CHARMM36m: an improved force field for folded and intrinsically disordered proteins. Nat Methods 14:71-73.

(42) Robustelli P, Piana S, Shaw DE (2018) Developing a molecular dynamics force field for both folded and disordered protein states. Proc Natl Acad Sci U S A. 115:E4758-E4766.

(43) Man VH, He X, Derreumaux P et al (2019) Effects of all-atom molecular mechanics force fields on amyloid peptide assembly: The case of $A\beta_{16-22}$ dimer. J Chem Theory Comput. 15:1440-1452.

(44) Barz B, Liao Q, Strodel B (2018) Pathways of amyloid-β aggregation depend on oligomer shape. J Am Chem Soc 140:319-327.

(45) Viet MH, Nguyen PH, Derreumaux P et al (2014) Effect of the English familial disease mutation (H6R) on the monomers and dimers of Aβ40 and Aβ42. ACS Chem Neurosci 5 : 646-657.

(46) Viet MH, Nguyen PH, Ngo ST et al (2013) Effect of the Tottori familial disease mutation (D7N) on the monomers and dimers of Aβ40 and Aβ42. ACS Chem Neurosci 4:1446-1457.

(47) Jang H, Arce FT, Ramachandran S et al (2014) Disordered amyloidogenic peptides may insert into the membrane and assemble into common cyclic structural motifs. Chem Soc Rev 43: 6750-6764.

(48) Zhang M, Ren B, Chen H et al (2017) Molecular simulations of amyloid structures, toxicity and inhibition. Isr. J. Chem 57: 586-601.

(49) Sahoo A., Matysiak S (2019) Computational Insights into Lipid Assisted Peptide Misfolding and Aggregation in Neurodegeneration. Phys Chem Chem Phys 21 : 22679-22694.

(50) Lindorff-Larsen K, Maragakis P, Piana S et al (2016) Picosecond to Millisecond Structural Dynamics in Human Ubiquitin. J Phys Chem B. 120:8313-820.

(51) Pan AC, Jacobson D, Yatsenko K et al (2019) Atomic-level characterization of protein-protein association. Proc Natl Acad Sci U S A 116:4244-4249.

(52) Xu L, Chen Y, Wang X (2014) Assembly of amyloid β peptides in the presence of fibril seeds: one-pot coarse-grained molecular dynamics simulations. J Phys Chem B. 118:9238-46.

(53) Pellarin R, Caflisch A (2006) Interpreting the aggregation kinetics of amyloid peptides. J. Mol. Biol. 360 : 882 – 892.

(54) Bellesia G, Shea J-E (2009) Effect of β-sheet propensity on peptide aggregation. J. Chem.Phys. 130 : 145103.

(55) Song W, Wei G, Mousseau N et al (2008) Self-assembly of the beta2-microglobulin NHVTLSQ peptide using a coarse-grained protein model reveals a beta-barrel species. J Phys Chem B. 112:4410-4418.

(56) Lu Y, Derreumaux P, Guo Z et al (2009) Thermodynamics and dynamics of amyloid peptide oligomerization are sequence dependent. Proteins. 75:954-963.

(57) Rojas AV, Maisuradze GG, Scheraga HA (2018) Dependence of the Formation of Tau and Aβ Peptide Mixed Aggregates on the Secondary Structure of the N-Terminal Region of Aβ. J Phys Chem B. 122 : 7049-7056.

(58) Ge X, Sun Y, Ding F (2018) Structures and dynamics of β-barrel oligomer intermediates of amyloid-beta16-22 aggregation. *Biochim Biophys Acta Biomembr.* 1860:1687-1697.

(59) Bunce SJ, Wang Y, Stewart KL et al (2019) Molecular insights into the surface-catalyzed secondary nucleation of amyloid-β_{40} ($A\beta_{40}$) by the peptide fragment $A\beta_{16-22}$. Sci Adv. 5:eaav8216.

(60) Urbanc B, Betnel M, Cruz, L et al. (2010) Elucidation of amyloid β-protein oligomerization mechanisms: discrete molecular dynamics study. J. Am. Chem. Soc. 132: 4266-4280.

(61) Popov KI, Makepeace KAT, Petrotchenko EV, Dokholyan NV, Borchers CH (2019) Insight into the structure of the unstructured tau protein. Structure. 27: 1710-1715.e4.

(62) Brodie NI, Popov KI, Petrotchenko EV, Dokholyan NV, Borchers CH (2019) Conformational ensemble of native alpha-synuclein in solution as determined by short-distance crossling constraint-guided discrete molecular dynamics simulations. PLos Comput Biol. 15(3): e1006859.

(63) Chiricotto M, Melchionna S, Derreumaux P et al (2019) Multiscale aggregation of the amyloid Aβ16–22 peptide: From disordered coagulation and lateral branching to Amorphous prefibrils. J. Phys. Chem. Lett 10:1594–1599.

(64) Brandner A, Timr S, Melchionna S et al (2019) Modelling lipid systems in fluid with Lattice Boltzmann Molecular Dynamics simulations and hydrodynamics. Sci Rep 9 : 16450.

(65) Granata D, Baftizadeh F, Habchi J et al (2015) The inverted free energy landscape of an intrinsically disordered peptide by simulations and experiments. Sci Rep 5:15449.

(66) Baftizadeh F, Biarnes X, Pietrucci F et al (2012) Multidimensional view of amyloid fibril nucleation in atomistic detail. J Am Chem Soc 134:3886-3894.

(67) Noé F, Olsson S, Kohler J, Wu, H (2019) Boltzmann generators: Sampling equilibrium states of many-body systems with deep learning. Science 365: eaaw1147.

(68) Tarus B, Tran TT, Nasica-Labouze J et al (2015) Structures of the Alzheimer's wild-type Aβ1-40 dimer from atomistic simulations. J Phys Chem B. 119 : 10478-10487.

(69) Nguyen PH, Sterpone F, Campanera JM et al (2016) Impact of the A2V mutation on the heterozygous and homozygous Aβ1-40 dimer structures from atomistic simulations. ACS Chem Neurosci 7: 823-832.

(70) Man VH, Nguyen PH, Derreumaux P (2017) High-Resolution Structures of the Amyloid-β 1-42 Dimers from the Comparison of Four Atomistic Force Fields. J Phys Chem B 121: 5977 – 5987.

(71) Nguyen PH, Tarus B, Derreumaux P (2014) Familial Alzheimer A2V mutation reduces the intrinsic disorder and completely changes the free energy landscape of the Aβ1-28 monomer. J Phys Chem B 118:501-510.

(72) Ngo ST, Nguyen PH, Derreumaux P (2020) Stability of Aβ11-40 Trimers with Parallel and Antiparallel β-Sheet Organizations in a Membrane-Mimicking Environment by Replica Exchange Molecular Dynamics Simulation. J Phys Chem B 124: 617 – 626.

(73) Hung HM, Nguyen MT, Tran P-T, Truong K, Chapman J, Anh LHQ, Derreumaux P, Vu VV, Ngo ST (2020) Impact of the Astaxanthin, Betanin and EGCG Compounds on Small Oligomers of the Amyloid Aβ40 Peptide. J Chem Inf Model 60:1399-1408.

(74) Zhang T, Xu W, Mu Y et al (2014) Atomic and dynamic insights into the beneficial effect of the 1,4-naphthoquinon-2-yl-L-tryptophan inhibitor on Alzheimer's Aβ1-42 dimer in terms of aggregation and toxicity. ACS Chem Neurosci 5:148-59.

(75) Nguyen P, Derreumaux P (2014) Understanding amyloid fibril nucleation and aβ oligomer/drug interactions from computer simulations. Acc Chem Res 47:603-611.

(76) Zhang T, Zhang J, Derreumaux P et al (2013) Molecular mechanism of the inhibition of EGCG on the Alzheimer Aβ(1-42) dimer. J Phys Chem B 117:3993-4002.

(77) Berthoumieu O, Nguyen PH, Castillo-Frias MP et al (2015) Combined experimental and simulation studies suggest a revised mode of action of the anti-Alzheimer disease drug NQ-Trp. Chemistry 21:12657-66.

(78) Jin Y, Sun Y, Chen Y, Lei J et al (2019) Molecular dynamics simulations reveal the mechanism of graphene oxide nanosheet inhibition of $A\beta_{1-42}$ peptide aggregation. Phys Chem Chem Phys 21:10981-10991.

(79) Fu Z, Luo Y, Derreumaux P et al (2009) Induced beta-barrel formation of the Alzheimer's Abeta25-35 oligomers on carbon nanotube surfaces: implication for amyloid fibril inhibition. Biophys J 97:1795-1803.

(80) Li H, Luo Y, Derreumaux P et al (2011) Carbon nanotube inhibits the formation of β-sheet-rich oligomers of the Alzheimer's amyloid-β(16-22) peptide. Biophys J 101:2267-2276.

(81) Nguyen PH, Campanera JM, Ngo ST et al (2019) Tetrameric Aβ40 and Aβ42 β-barrel structures by extensive atomistic simulations. I. In a bilayer mimicking a neuronal Membrane. J Phys Chem B 123:3643-3648.

(82) Nguyen PH, Campanera JM, Ngo ST et al (2019) Tetrameric Aβ40 and Aβ42 β-barrel structures by extensive atomistic simulations. II. In aqueous solution. J Phys Chem B 123: 6750-6756.

(83) Ngo ST, Nguyen PH, Derreumaux P (2020) Impact of A2T and D23N Mutations on Tetrameric Aβ42 Barrel Within a Dipalmitoylphosphatidylcholine Lipid Bilayer Membrane by Replica Exchange Molecular Dynamics. J Phys Chem B 124: 1175 – 1182.

(84) Tuffery P, Derreumaux P (2012) Flexibility and binding affinity in protein-ligand, protein-protein and multi-component protein interactions: limitations of current computational approaches. J R Soc Interface 9:20-33.

(85) Nasica-Labouze J, Meli M, Derreumaux P, et al (2011) A multiscale approach to characterize the early aggregation steps of the amyloid-forming peptide GNNQQNY from the yeast prion sup-35. PLoS Comput Biol 7:e1002051.

(86) Smith AK, Lockhart C, Klimov DK (2016) Does replica exchange with solute tempering efficiently sample Aβ peptide conformational ensembles? J Chem Theory Comput 12 : 5201-5214.

(87) Dominguez L, Foster L, Straub JE et al (2016) Impact of membrane lipid composition on the structure and stability of the transmembrane domain of amyloid precursor protein. Proc Natl Acad Sci U S A 113:E5281-5287.

(88) Nguyen HL, Krupa P, Hai NM et al (2019) Structure and Physicochemical Properties of the Aβ42 Tetramer: Multiscale Molecular Dynamics Simulations. J Phys Chem B 123(34):7253-7269.

(89) Chebaro Y, Jiang P, Zang T et al (2012) Structures of Aβ17-42 trimers in isolation and with five small-molecule drugs using a hierarchical computational procedure. J Phys Chem B 116:8412-8422.

(90) Cote Y, Delarue P, Scheraga HA, Senet P, Maisuradze GG (2018) From a Highly Disordered to a Metastable State: Uncovering Insights of α-Synuclein. ACS Chem Neurosci 9: 1051 – 1065.

(91) Marinari E, Parisi G (1992) Simulated Tempering: A New Monte Carlo Scheme. Europhys. Lett. 19: 451-458.

(92) A. Irback A, Potthast F (1995) Studies of an off-lattice model for protein folding: Sequence dependence and improved sampling at finite temperature. J. Chem. Phys 103 :10298-10305.

(93) Hansmann UHE, Okamoto Y (1997) Numerical comparisons of three recently proposed algorithms in the protein folding problem. J. Comput. Chem 18: 920-933.

(94) Park S, Pande, VS (2007) Choosing weights for simulated tempering. Phys. Rev. E. 76: 017603.

(95) Mitsutake A, Okamoto Y (2000) Replica-exchange simulated tempering method for simulations of frustrated systems. Chem. Phys. Lett 332: 131-138.

(96) Mitsutake A, Okamoto Y (2004) Replica-exchange extensions of simulated tempering method. J. Chem. Phys 121: 2491-2504.

(97) Mitsutake A, Okamoto Y (2009) Multidimensional generalized-ensemble algorithms for complex systems. J. Chem. Phys 130: 214105.

(98) Favrin G, Irback A, Mohanty S (2004) Oligomerization of amyloid Aβ16-22 peptides using hydrogen bonds and hydrophobicity forces. Biophys. J 87: 3657-3664.

(99) Nguyen PH, Okamoto Y, Derreumaux P (2013) Simulated tempering with fast on-the-fly weights determination. J. Chem. Phys 138: 061102.

(100) Zhang T, Nguyen PH, Nassica-Labouze J et al (2015) Folding atomistic proteins in explicit solvent using simulated tempering. J. Phys. Chem. B 119: 6941-6951.

(101) Nguyen PH, Li MS, Derreumaux P (2011) Effects of all-atom force fields on amyloid oligomerization: replica exchange molecular dynamics simulations of the Aβ(16-22) dimer and trimer. Phys Chem Chem Phys 13:9778-9788.

(102) Viet MH, Derreumaux P, Nguyen PH (2015) Multiple atomistic force fields in a single advanced sampling simulation. J. Chem. Phys 143: 021101.

(103) Doig AJ, Del Castillo-Frias MP, Berthoumieu O et al (2017) Why is research on amyloid-β failing to give new drugs for alzheimer's disease? ACS Chem Neurosci 8:1435-1437

(104) Smith JF, Knowles TP, Dobson CM et al (2006) Characterization of the nanoscale properties of individual amyloid fibrils. Proc. Natl. Acad. Sci. U.S.A 103 :15806-15811.

(105) Fitzpatrick AW, Vanacore GM, Zewail AH (2015) Nanomechanics and intermolecular forces of amyloid revealed by four-dimensional electron microscopy. Proc. Natl. Acad. Sci. U. S. A 112: 3380-3385.

(106) Reches M, Gazit E (2003) Castingmetal nanowires within discrete self-assembled peptide nanotubes. Science 300: 625-627.

(107) Booth DR, Sunde M, Bellotti V et al (1997) Instability, unfolding and aggregation of human lysozyme variants underlying amyloid fibrillogenesis. Nature 385: 787-793.

(108) Waldauer SA, Hassan S, Paoli B et al (2012) Photocontrol of Reversible Amyloid Formation with a Minimal-Design Peptide. J. Phys. Chem B 116: 8961.

(109) Johny M, Vijayalakshmi K, Das A et al (2017) Modulating the Phe–Phe dipeptide aggregation landscape via covalent attachment of an azobenzene photoswitch. Chem Comm 53: 9348.

(110) Deeg AA, Schrader TE, Kempter S et al (2011) Light-Triggered Aggregation and Disassembly of Amyloid-Like Structures. ChemPhysChem 12: 559.

(111) Measey TJ, Gai F (2012) Light-Triggered Disassembly of Amyloid Fibrils. Langmuir 28: 34.

(112) Kawasaki T, Fujioka J, Imai T et al (2014) Mid-infrared free-electron laser tuned to the amide I band for converting insoluble amyloid-like protein fibrils into the soluble monomeric form. Lasers in Medical Science 29: 1701-1707.

(113) Kawasaki T, Fujioka J, Imai T et al (2012) Effect of Mid-infrared Free-Electron Laser Irradiation on Refolding of Amyloid-Like Fibrils of Lysozyme into Native Form. The Protein Journal 31: 710-716.

(114) Kawasaki T, Imai T, Tsukiyama K (2014) Use of a Mid-Infrared Free-Electron Laser (MIR-FEL) for Dissociation of the Amyloid Fibril Aggregates of a Peptide. Journal of Analytical Sciences, Methods and Instrumentation, 4 : 9-18.

(115) Kawasaki T, Yaji T, Imai T et al (2014) Synchrotron-Infrared Microscopy Analysis of Amyloid Fibrils Irradiated by Mid-Infrared Free- Electron Laser. American Journal of Analytical Chemistry, 5 : 384-394.

(116) Leinenga G, Gotz J (2015) Scanning ultrasound removes amyloid-β and restores memory in an Alzheimer's disease mouse model. Science Translational Medicine 7: 278ra33.

(117) Chatani E, Lee YH, Yagi H et al (2009) Ultrasonication-dependent production and breakdown lead to minimum-sized amyloid fibrils. Proc. Natl. Acad. Sc. U.S.A 106: 1119.

(118) Yagi H, Hasegawa K, Y. Yoshimura Y et al (2009) Acceleration of the depolymerization of amyloid β fibrils by ultrasonication. Biochimica et Biophysica Acta. 1834: 2480-2485.

(119) Viet MH, Derreumaux P, Li MS et al (2015) Picosecond dissociation of amyloid fibrils with infrared laser: a nonequilibrium simulation study. J. Chem. Phys 143: 155101.

(120) Viet MH, Truong PM, Derreumaux P et al (2015) Picosecond melting of peptide nanotubes using an infrared laser: a nonequilibrium simulation study. Phys. Chem. Chem. Phys 17: 27275.

(121) Viet MH, Nguyen VO, Derreumaux P et al (2016) Picosecond infrared laser-induced all-atom nonequilibrium molecular dynamics simulation of dissociation of viruses. Phys. Chem. Chem. Phys 18: 11951.

(122) Domin D, Viet MH, Nguyen-Thi VO et al (2018) Breaking down cellulose fibrils with a mid-infrared laser. Cellulose 25: 5553–5568.

(123) Botan V, Backus EHG, Pfister R et al (2007) Energy transport in peptide helix. Proc. Natl. Acad. Sci. U.S.A. 104: 12749.

(124) Kawasaki T, Man Viet, Sugimoto Y, S Nobuyuki, Yamamoto H, Tsukiyama K, Wang J, Derreumaux P, Nguyen P. (2020) Infrared Laser Induced Amyloid Fibril Dissociation: A Joint Experimental/Theoretical Study on the GNNQQNY Peptide. J. Phys. Chem. B doi:101021/acs.jpcb.0c05385.

(125) Derreumaux P, Vergoten, G (1995) A new spectroscopic molecular mechanics force field. Parameters for proteins. J. Chem. Phys. 102, 8586.

(126) Okumura H, Itoh SG (2014) Amyloid fibril disruption by ultrasonic cavitation: nonequilibrium molecular dynamics simulations. J Am Chem Soc 136 :10549-10552.

(127) Man VH, Derreumaux P, Nguyen PH (2016) Nonequilibrium all-atom molecular dynamics simulation of the ultrasound induced bubble vibration and application to dissociate amyloid fibrils. J. Chem. Phys 145: 174113.

(128) Man VH, Derreumaux P, Nguyen PH (2018) Rayleigh-Plesset equation of the bubble stable cavitation in water: a nonequilibrium all-atom molecular dynamics simulation study. J. Chem. Phys. 148: 094505.

(129) Ilie IM, Caflisch A (2019) Simulation studies of amyloidogenic polypeptides and their aggregates. *Chem Rev* 119: 6956 – 6993.

(130) Nguyen PH, Sterpone F, Derreumaux P (2020) Aggregation of disease-related peptides. Prog Mol Biol Transl Sci. 170:435-460.

(131) Derreumaux P, Man VH, Wang J, Nguyen PH (2020) Tau R3-R4 Domain Dimer of the Wild Type and Phosphorylated Ser356 Sequences. I. In Solution by Atomistic Simulations. J Phys Chem B. 124:2975-2983.

(132) Cao Y, Tang X, Yuan M, Han W (2020) Computational studies of protein aggregation mediated by amyloid: Fibril elongation and secondary nucleation. Prog Mol Biol Transl Sci. 170:461-504.

(133) Nam HB, Kouza M, Zung H, Li MS (2010) Relationship between population of the fibril-prone conformation in the monomeric state and oligomer formation times of peptides: Insights from all-atom simulations. J. Chem. Phys. 132, 165104.

(134) Chebaro Y, Pasquali S, Derreumaux P (2012) The coarse-grained OPEP force field for non-amyloid and amyloid proteins. J Phys Chem B. 116:8741-8752.

(135) Sterpone F, Nguyen PH, Kalimeri M et al (2013) Importance of the ion-pair interactions in the OPEP coarse-grained force field: parametrization and validation. J Chem Theory Comput 9: 4574-4584.

(136) Zhang Y, Liu H, Yang S, Luo R, Chen H-F (2019) Well-Balanced Force Field *ff*03*CMAP* for Folded and Disordered Proteins. J Chem Theory Comput. 15, 6769 – 6780.

(137) Shabane PS, Izadi S, Onufriev AV (2019) General purpose water model can improve atomistic simulations of intrinsically disordered proteins. J Chem Theory Comput. 15, 2620 – 2634.

(138) Pietrek LM, Stelzl LS, Hummer G (2020) Hierarchical Ensembles of Intrinsically Disordered Proteins at Atomic Resolution in Molecular Dynamics Simulations. J Chem Theory Comput. 16:725-737.

(139) Shen Y, Maupetit J, Derreumaux P, Tufféry P (2014) Improved PEP-FOLD Approach for Peptide and Miniprotein Structure Prediction. J Chem Theory Comput. 10:4745-58.

(140) Lu Y, Shi XF, Nguyen PH, Sterpone F, Salsbury FR Jr, Derreumaux P (2019) Amyloid-β(29-42) Dimeric Conformations in Membranes Rich in Omega-3 and Omega-6 Polyunsaturated Fatty Acids. J Phys Chem B. 123:2687-2696.

(141) Sterpone F, Derreumaux P, Melchionna S (2018) Molecular Mechanism of Protein Unfolding under Shear: A Lattice Boltzmann Molecular Dynamics Study. J Phys Chem B. 122:1573-1579.

(142) Chiricotto M, Sterpone F, Derreumaux P, Melchionna S (2016) Multiscale simulation of molecular processes in cellular environments. Philos Trans A Math Phys Eng Sci. 374:2080.

(143) Lu Y, Shi XF, Salsbury FR Jr, Derreumaux P (2018) Influence of electric field on the amyloid-β(29-42) peptides embedded in a membrane bilayer. J Chem Phys. 148:045105.

(144) Mioduszewski L, Cieplak M (2018) Disordered peptide chains in an alpha-C-based coarse-grained model. Phys. Chem. Chem. Phys. 20:19057-19070.

(145) Mioduszewski L, Cieplak M (2020) Protein droplets in systems of disordered homopeptides and the amyloid glass phase. Phys. Chem. Chem. Phys. 22:15592-15599.

(146) Mioduszewski L, Rozycki B,Cieplak M (2020) Pseudo-improper-dihedral model for intrinsically disordered proteins. J. Chem. Theor. Comput. 16:4726-4733.

(147) Nguyen PH, Derreumaux P (2020) Structures of the intrinsically Aβ, tau and α -synuclein proteins in aqueous solution from computer simulations. Biophys. Chem. 264:106421.

(148) Doig AJ, Derreumaux P (2015) Inhibition of protein aggregation and amyloid formation by small molecules. Curr Opin Struct Biol. 3: 50-56.

(149) Mahul-Mellier AL, Burtscher J, Maharjan N, Weerens L, Croisier M, Kuttler F, Leleu M, Knott GW, Lashuel HA (2020) The process of Lewy body formation, rather than simply α-synuclein fibrillization, is one of the major drivers of neurodegeneration. Proc Natl Acad Sci U S A. 117:4971-4982.

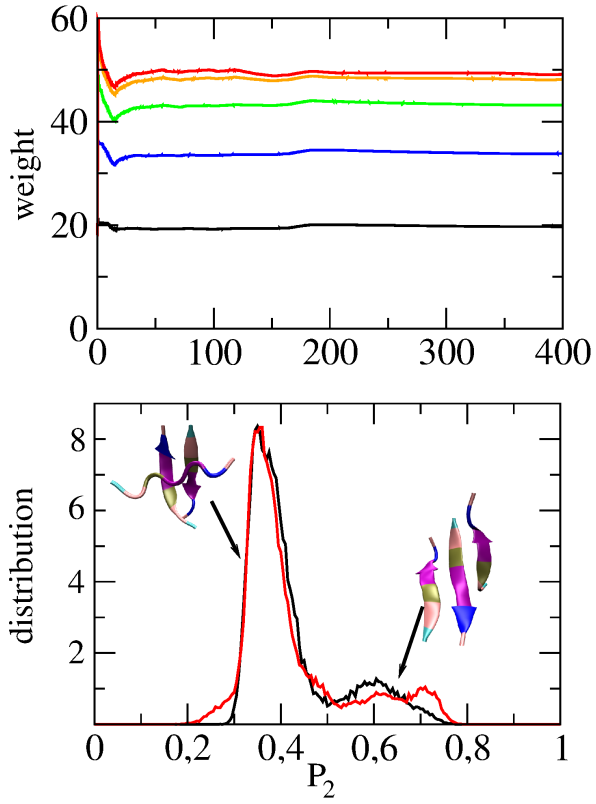

Figure 1. Time evolution of the weights (above) and the distribution of the order parameter P_2 at T = 300 K (below) obtained from ST simulation (black) and from REMD (red). The representative structures corresponding to the two dominant peaks are also shown.

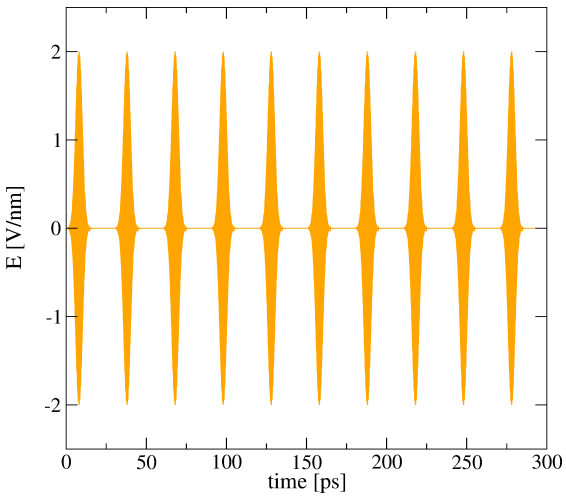

Figure 2. Chain of laser pulses with frequency $\omega = 1355\ cm^{-1}$, $E_0 = 2Vnm^{-1}$ and separated by 50 ps.

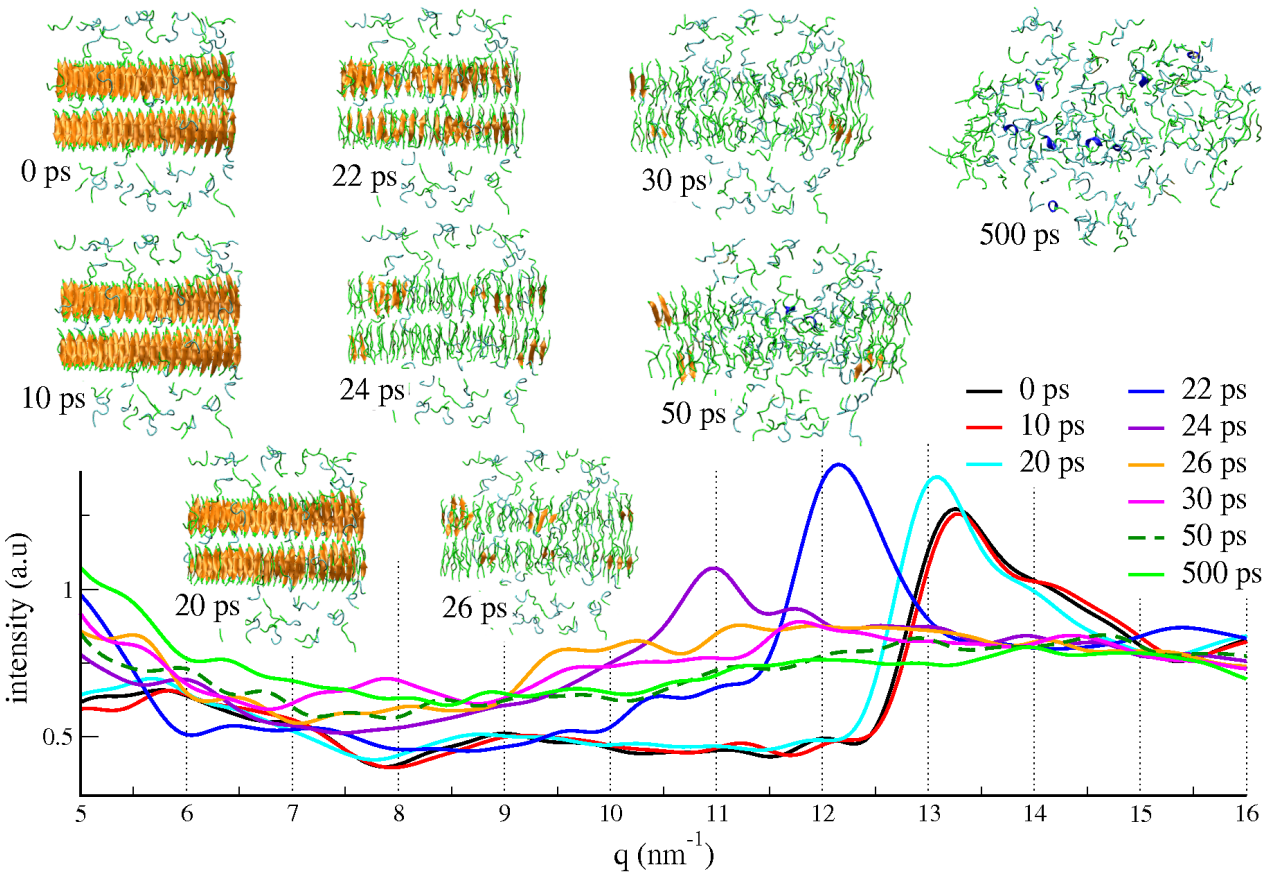

Figure 3. Snapshots of the system at selected times during the NEMD simulations and corresponding WAXS spectra.

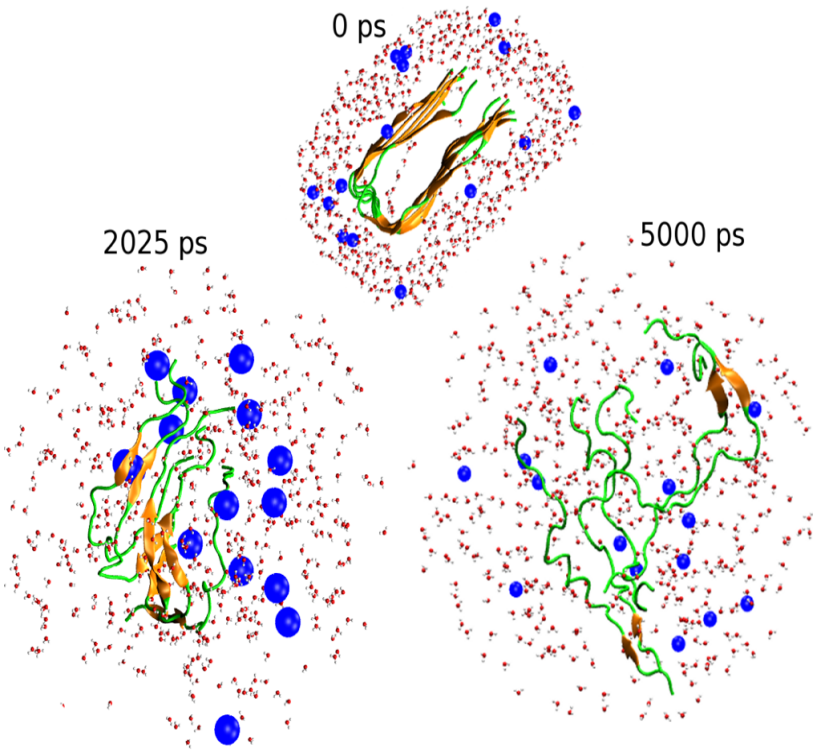

Figure 4. The initial structure of the fibril (0 ps) and two selected snapshots at 2025 ps and 5000 ps, where the bubbles (blue spheres) reach the maximum and minimum radii, respectively. For clarity, only a cross section and some selected waters, bubbles (blue spheres) are shown.